Identifying tsunami traces beyond sandy tsunami deposits using terrigenous biomarkers: a case study of the 2011 Tohoku-oki tsunami in a coastal pine forest, northern Japan

Tetsuya Shinozaki (tetsuya.shinozaki@aist.go.jp)
National Institute of Advanced Industrial Science and Technology Geological Survey of Japan: Sangyo Gijutsu Sogo Kenkyujo Chishitsu Chosa Sogo Center https://orcid.org/0000-0002-8991-5973

Yuki Sawai
National Institute of Advanced Industrial Science and Technology Geological Survey of Japan: Sangyo Gijutsu Sogo Kenkyujo Chishitsu Chosa Sogo Center

Minoru Ikehara
Kochi University: Kochi Daigaku

Dan Matsumoto
National Institute of Advanced Industrial Science and Technology Geological Survey of Japan: Sangyo Gijutsu Sogo Kenkyujo Chishitsu Chosa Sogo Center

Yumi Shimada
National Institute of Advanced Industrial Science and Technology Geological Survey of Japan: Sangyo Gijutsu Sogo Kenkyujo Chishitsu Chosa Sogo Center

Koichiro Tanigawa
National Institute of Advanced Industrial Science and Technology Geological Survey of Japan: Sangyo Gijutsu Sogo Kenkyujo Chishitsu Chosa Sogo Center

Toru Tamura
National Institute of Advanced Industrial Science and Technology Geological Survey of Japan: Sangyo Gijutsu Sogo Kenkyujo Chishitsu Chosa Sogo Center

Research Article

Keywords: 2011 Tohoku-oki tsunami, Grain-size analysis, Biomarker, Coastal forest

Posted Date: March 8th, 2022

DOI: https://doi.org/10.21203/rs.3.rs-1417239/v1

Abstract

The distributions of sandy tsunami deposits do not reflect the true extents of tsunami inundation areas, leading to underestimates of inundation by past tsunamis and thus the magnitudes of their associated tsunamigenic earthquakes. To archive the sedimentological and geochemical features of the 2011 Tohoku-oki tsunami deposit, we performed visual observations and computed-tomography, grain-size, water content, and organic geochemical analyses of sediments from a coastal forest at Oirase Town, northern Japan. Stratigraphic observations revealed the 2011 tsunami deposit to be a landward-thinning interbedded sand and soil layer that became ambiguous in landward locations. The sediment samples from the inundated area did not contain marine-sourced biomarkers; instead, peak concentrations of isolongifolene, an organic compound derived from *Pinus* in the forest, were observed within or just above the sandy tsunami deposits in sediment sections. Peak isolongifolene concentrations were also detected in landward soils inundated by the tsunami in which no sand layer was observable, but were not observed beyond the inundation limit. Although this characteristic biomarker is unique to this and similar depositional environments, these results suggest that lateral changes of the concentrations of environment-specific biological proxies in the sedimentary column may record tsunami inundation.

1 Introduction

Large tsunamis triggered by subduction-zone earthquakes occur on time scales of 100–1,000 years (e.g., Paris et al. 2020), representing a low-frequency, catastrophic natural disaster recurring on human time scales. Current instrumental records date back only about 100 years and archival records not more than 1,000 years in most parts of the world (Satake and Atwater 2007). Tsunami deposits are thus particularly important because they record events predating historical records. Indeed, the spatial distributions and chronologies of tsunami deposits have been used to reconstruct the magnitudes and recurrence intervals of tsunamis and earthquakes in tectonically active margins (e.g., Atwater et al. 2005; Jankaew et al. 2008; Fujiwara et al. 2020; Goff et al. 2020; Sawai 2020; Costa et al. 2021).

Studies comparing the inundation area of the 2011 Tohoku-oki tsunami with the maximum landward extent of the associated sandy deposits indicate that sandy tsunami deposits are not always preserved in inundation areas (Goto et al. 2011; Abe et al. 2012, 2020). For example, Abe et al. (2012) reported that sandy tsunami deposits ≥ 0.5 cm thick are distributed over only 57–76% of inundated areas, especially in areas where the tsunami ran up > 2.5 km inland. Therefore, tsunamis do not transport sand to the landward inundation limit and the distributions of sandy tsunami deposits likely underestimate the inundation limits of past tsunamis and thus the magnitudes of their associated tsunamigenic earthquakes (Sawai et al. 2012; Namegaya and Satake 2014). To more precisely reconstruct past tsunami events, it is therefore necessary to establish a method of accurately identifying their inundation areas.

Only a handful of previous studies have sought geochemical proxies to reveal tsunami traces lacking observable sand deposits. For example, high concentrations of seawater components such as chloride

and sulphate were detected in coastal lowlands beyond the extents of sandy deposits from the 2010 Maule (Chagué-Goff et al. 2015) and 2011 Tohoku-oki tsunamis (Goto et al. 2011; Chagué-Goff et al. 2012). Moreira et al. (2017) also detected salinity indicators such as Cl and Br beyond the inland limits of sandy deposits from the 1755 Lisbon tsunami and accordingly re-estimated the inundation distance. Nonetheless, other geochemical proxies of tsunami traces beyond the landward limits of sandy deposits remain largely unexplored and further case studies should explore various approaches that are appropriate for different coastal settings and inundation events.

A coastal forest in Oirase Town, northern Japan, was partly inundated by the 2011 Tohoku-oki tsunami and thus provides an opportunity to apply geochemical proxies for detecting tsunami inundation events. We therefore performed grain-size and organic geochemical analyses of sediment samples collected from this coastal forest in search of such proxies.

2 Study Site

2.1 Geomorphology

Our study site is a coastal forest facing the Pacific Ocean in Oirase Town, Aomori Prefecture, northern Japan (Fig. 1a, b). Landward from the ocean, the Oirase area consists of a sandy beach 100–150 m wide and a coastal pine forest 100–200 m wide (Fig. 1c). The beach and coastal forest were separated by a seawall approximately 6 m high before the 2011 Tohoku-oki tsunami; for greater protection from inundation, the height of the seawall was subsequently increased to 7 m (Fig. 1d, e). The former coastal forest was heavily damaged by the tsunami associated with the M 8.1 1933 Showa-Sanriku earthquake (Utsu 2004) and pine trees were replanted after that event (Nakamura et al. 2012).

2.2 The 2011 Tohoku-oki tsunami and associated tsunami deposit

Three tsunami waves struck the study area during the 2011 Tohoku-oki tsunami, the second being the largest (Koiwa et al. 2014). The run-up and inundation heights in this area were 5.3 and 4.5 m, respectively (Fig. 1c; The 2011 Tohoku Earthquake Tsunami Joint Survey Group 2011). Several studies have investigated the associated tsunami deposit in this area. Nakamura et al. (2012) reported local variations in tsunami inundation and the sedimentary characteristics and component minerals of the 2011 Tohoku-oki tsunami deposit; they found that the tsunami deposits were mainly affected by coastal topography and the extent of erosion at any one point, rather than by flow height. Koiwa et al. (2014) examined the tsunami behavior based on interpretations of sequential digital photographs of the tsunami, the spatial distribution of tsunami deposits, and topography reconstructed using a digital elevation model. Both studies found that the thick tsunami deposits comprise multiple unlaminated layers with inverse and normal grading. These layers probably formed by repeated accelerations and decelerations during the several minutes between the arrival of the tsunami and the start of the backwash flow (Koiwa et al. 2014).

Tanigawa et al. (2018) conducted a field survey around the Oirase coastal forest several months after the 2011 tsunami and examined the source of transported sand based on the diatom assemblages. They concluded that the sand in the deposit was sourced from sub-, inter-, and supratidal (including beach and dune) sediments. In addition, they reported the tsunami inundation limit based on eyewitness accounts and the distribution of debris (Fig. 1c).

Bellanova et al. (2021) traced a wood- and organic-bearing deposit directly atop the sandy deposit; it extended further inland than the sandy deposit, and they accordingly re-estimated the extent of the tsunami inundation area. They also determined sediment sources based on biological and anthropogenic proxies and depth profiles of the terrigenous/aquatic ratio, which indicates relative amounts of terrestrial versus aquatic *n*-alkanes in a sediment (Peters et al. 2007). They found that the wood- and organic-rich tsunami trace showed less onshore and more marine signals than the soil and dune sediments. In addition, the 16 priority pollutant polycyclic aromatic hydrocarbons, which are anthropogenic markers, were present at high concentrations in the tsunami sand deposit and pre-tsunami soil and dune sediments.

3 Methods

In October 2020, we collected sediment samples within the area of the coastal forest inundated by the 2011 tsunami along two transects roughly perpendicular to the shoreline (Figs. 1c–e, 2). Sediment samples were taken directly from the walls of excavated pits using a 18-cm-long and 10-cm-wide plastic box (Fig. 2b, c) at seven locations along Transect A (A1–A7) and five along Transect B (B1–B5) (Fig. 1d, e). The sediment samples were visually described and photographed. We also collected a reference sediment sample (R, Fig. 1c) beyond the known inundation limit in June 2021 using the same sampling approach. In addition, pine bark, needles, and cones on the ground surface were collected for geochemical reference data. Topography was measured using a Leica Viva TS15 imaging total station (Leica Geosystems, St. Gallen, Switzerland) and a Leica Viva GS10 high-precision GNSS receiver.

In the laboratory, sediment samples were scanned using a computed tomography (CT) scanner (Supria Grande, Hitachi) in the Geological Survey of Japan laboratory (National Institute of Advanced Industrial Science and Technology). They were then subsampled in 1-cm-thick vertical intervals. The subsamples were dried at 60°C for 24 h, and their water contents (%) were calculated from the sample weights before and after drying. A portion of the dried samples was then homogenized with an agate mortar and pestle, weighed, and ashed at 550°C for 4 h to estimate loss on ignition (LOI550, %), which is indicative of organic content (Dean 1974; Santisteban et al. 2004).

Before grain-size analysis, organics and carbonates were respectively removed from the remaining dried samples by dissolution in hydrogen peroxide (H_2O_2) and hydrochloric acid (HCl). The samples were then sieved at 63 μm (4 phi) to remove the mud fraction, and the sand content (%) was calculated from the sample weights before and after sieving. Grain-size analysis was performed on the residual sand samples using an image analyzer (Camsizer, Retsch Technology GmbH, Haan, Germany) with an

effective measuring range of − 5.25 phi (pebble) to 6.25 phi (silt) at 0.25-phi intervals. The mean grain size of each sample was then calculated from the measurements using the logarithmic graphical method of Folk and Ward (1957).

We kept about 1.9–2.4 g of each subsample from location A6 for radioactive cesium measurements using a gamma spectrometer at the Geological Survey of Japan (GCW2022, Canberra Industries Inc., USA). The ^{137}Cs ($t_{1/2}$ = 30.2 years) data were used to detect horizons of specific ages (e.g., 1950–1964 CE; He and Walling 1997; Wren and Davidson 2011).

Biomarkers were measured in samples A1, A4, A6, A7, and the reference sample, as well as in the pine materials taken from the ground surface. Because large plant fragments constitute a large portion of the organic matter present in these sediments (Shinozaki 2021), terrestrial plants were mostly removed from each subsample using a 250-μm sieve, and fraction finer than 250-μm in each subsample was then dried and homogenized. Lipids were extracted from the homogenized subsamples with dichloromethane and methanol using an accelerated solvent extractor (ASE350, Dionex, Sunnyvale, USA). Hydrocarbons (N1 fraction; locations A1, A2, A4, A6, R, and pine materials), ketones (N3; locations A4 and A6 only), and alcohols and sterols (N4; locations A4 and A6 only) were extracted as described by Shinozaki et al. (2015). These organic fractions were measured using a gas chromatograph with flame-ionization detection (Agilent 7890B or Agilent 6890N, Agilent Technologies Inc., USA) and an Agilent DB-5HT nonpolar column (30 m long, 0.25 mm internal diameter). Individual compounds were identified using an Agilent 5973 network mass selective detector gas chromatograph/mass spectrometer (GC-MS).

4 Results

4.1 Sedimentological characteristics

4.1.1 Transect A

At most locations, the sediment samples consisted of an upper organic soil layer that contained sand particles and a thick lower fine- to medium-grained sand layer (A2–A7, Fig. 3). Based on visual observations, fine- to medium-grained sand layers 1.5–4.0 cm thick were intercalated into the soil layer at locations A1, A2, A4, and A5, but could not be identified within the soil layer at locations A3, A6, and A7 (Fig. 3). The intercalated sand layer thinned landward (Fig. 3). The contacts between the sand and soil layers were vague, especially at inland locations A4 and A5. No sedimentological structure was observed in the intercalated sand layer. At location A1, the intercalated sand contained abundant colorless minerals. The soil, intercalated sand layer, and upper part of the bottom sand layer contained fine roots (Fig. 3).

In the CT images, the sand layers at locations A1, A2, and A4 were easily identifiable, but those at locations A3 and A5–A7 were difficult to identify, if present at all (Fig. 3). At locations A1, A2, and A4, the positions of the intercalated sand layers in the CT images corresponded to those observed visually.

Water content and LOI550 showed similar trends, both being relatively high in the soil layer and low in the bottom and intercalated sand layers (Fig. S1). Notably, both were highest at the top of the soil and decreased with increasing depth (Fig. S1). At locations A1 and A4, these values markedly decreased within the intercalated sand layer, but at locations A2 and A5, these values only slightly decreased within the intercalated sand layer. As with the CT images, the water content and LOI550 depth profiles did not show any remarkable features in the soil layer at the most landward locations (A6 and A7, Fig. S1).

Sand content was generally low at the top of the soil layer and tended to increase with increasing depth (Fig. S2). The bottom sand layer contained > 80% sand (Fig. S2). Sand contents in the soil layer at seaward locations were > 50%, but that at the most inland location (A7) was only 12%. Mean grain size was generally finer and more variable in the soil layer than in the bottom sand layer (Fig. S2), although there were some differences among the trends at different locations. For example, we observed small variations of the mean grain size in the soil and sand layers at location A3 and large variations in the lower sand layer at location A4 (Fig. S2).

The soil layer was poorly sorted, especially in the upper part (Fig. S3), whereas the bottom sand layer was well sorted with no significant variation with depth (Fig. S3). At all locations, it was difficult to discriminate the intercalated sandy layer from the soil layer based on the depth profiles of the grain-size distribution (Fig. S3).

4.1.2 Transect B

Sediments from Transect B also consisted of an upper organic soil layer atop a thick fine- to medium-grained sand layer (B1–B5, Fig. 3). Fine- to medium-grained sand layers 0.5–3.0 cm thick intercalated into the soil layer were visually identifiable at locations B1–B4, but we could not identify an intercalated sand layer at location B5 (Fig. 3). At locations B3 and B4, the intercalated sand was not layered, but only partially contained within the soil. The intercalated sand layer thinned landward (Fig. 3). No sedimentological structure was observed in the intercalated sand layer. Fine roots were present in the soil, the intercalated sand layers, and the upper part of the bottom sand layer (Fig. 3).

In CT images, the intercalated sand layers could be identified within the soil at locations B1 and B2, but those at locations B3–B5, if present, were difficult to identify (Fig. 3). At locations B1 and B2, the positions of the intercalated sand layers in the CT images corresponded to those observed visually.

Within the soil layer, water content and LOI550 were highest at the top and gradually decreased within increasing depth (Fig. S1); values in the bottom sand layer were stable and low. The water content and LOI550 values in the intercalated sand layers at locations B1 and B2 were similar to those in the bottom sand layers (Fig. S1).

Sand contents were generally low at the top of the soil layer and increased with increasing depth toward the bottom sand layer (Fig. S2), which contained > 80% sand (Fig. S2). The mean grain size was fine at the top of the soil layer, gradually coarsened with depth, and was fairly stable in the bottom sand layer (Fig. S2).

The soil layer, especially its upper part, was poorly sorted (Fig. S3), whereas the bottom sand layer was consistently well sorted (Fig. S3). At all locations, it was difficult to identify the intercalated sand layer based on the depth profiles of the grain-size distribution (Fig. S3).

4.2 Biomarkers

We illustrate the N1 (hydrocarbon) chromatographs for location A4 (Fig. 4), which are generally representative of those at other locations. At locations A1, A4, A6, A7, and R, long-chain *n*-alkanes (C_{23}–C_{33}) were detected in every measured layer. The peaks of odd-numbered *n*-alkanes (C_{23}–C_{33}) were larger than those of even-numbered *n*-alkanes (C_{24}–C_{32}), primarily reflecting contributions from vascular plants (Eglinton and Hamilton, 1963). None of the samples contained detectable short-chain *n*-alkanes (C_{15}–C_{19}).

A significant peak was observed at a retention time of ca. 6.3 min in all layers and at all measured locations; analysis by a GC-MS identified this peak as isolongifolene ($C_{15}H_{24}$), a main sesquiterpene component derived from an essential oil of pine. For example, sesquiterpene in the essential oil of *Pinus thunbergii* heart wood contains 30.5% longifonene (Mukai et al. 2017). Indeed, the analyzed pine bark, needles, and cones taken from the ground surface contained isolongifolene at concentrations on the order of 10^4–10^5 ng/g. Background isolongifolene concentrations in the soil layers at locations A1, A4, A6, A7, and R were typically less than 2.5×10^3 ng/g (Fig. 5), consistent with the location of the study site in a coastal pine forest (Figs. 1c, 2a). Isolongifolene concentrations well above the background in the depth profiles appear to correlate with inundation by the 2011 Tohoku-oki tsunami (Fig. 5). Peaks at locations A1 and A4 occur just above and within the sandy tsunami deposits, respectively, whereas concentrations do not exceed the background at the reference site (Fig. 5).

At locations A4 and A6, alkenones (long-chain C_{37}–C_{39} unsaturated methyl and ethyl ketones derived from several species of haptophytes, primarily oceanic phytoplankton including the widely distributed coccolithophorids *Emiliania huxleyi* and *Gephyrocapsa oceanica*; Volkman et al. 1980; Marlowe et al. 1984; Conte et al. 1994) were not detected in any samples. Sterols (cholesterol and phytosterols such as stigmasterol and β-sitosterol) were detected as components of the N4 fraction in every measured layer, but no marine-sourced sterols, such as dinosterol or brassicasterol, were detected in any layer at these locations.

5 Discussion

5.1 Discrepancy between tsunami inundation area and the distribution of sandy tsunami deposits

We interpret the sand layer intercalated in the soil layer as the 2011 Tohoku-oki tsunami deposit. A sandy organic soil has developed at the study site after the replanting of pine trees in 1933 (Nakamura et al. 2012). Therefore, the tsunami sand deposited on the ground surface in 2011 (Tanigawa et al. 2018) is

easily recognizable as the intercalated sand layer, which has since been covered by organic soil that developed under normal depositional conditions. We could only trace the sandy tsunami deposits as far inland as locations A5 and B4 (222.3 and 217.6 m from the present shoreline, respectively; Fig. 3), about 78% of the total inundation distance (280 m from the present shoreline according to Tanigawa et al. 2018).

5.2 Terrigenous biomarker distribution consistent with the inundation area

Sedimentological and standard geochemical approaches did not provide any evidence for a marine incursion as far inland as the known limit of tsunami inundation. Beyond the sandy tsunami deposit (locations A6, A7, and B5; Figs. S1–S3), it was difficult to identify the event layer from sedimentological approaches alone (CT images, sand content, mean grain size, and grain-size distribution). Furthermore, our biomarker analysis failed to detect any marine-sourced biomarkers, such as short-chain *n*-alkanes, alkenones, dinosterol, and brassicasterol, both at locations where the sandy tsunami deposit was (A1, A4) and was not recognized (A6, A7; Fig. 4). Indeed, marine-sourced biomarkers tend to adsorb onto organic-rich, fine-grained particles (Shinozaki et al. 2015), and it is therefore likely that these biomarkers were too scarce to be detected in the coastal forest zone near the shoreline.

One striking result of our geochemical analysis, however, is that elevated isolongifolene concentrations were observed at every location within the inundation area (Fig. 4). At location A1, the peak concentrations may be due to the accumulation of isolongifolene in a mud cap generated by the tsunami waves and/or the tsunami waves physically impacting the trees and knocking loose pine materials to the ground. Although it is not clear why the isolongifolene concentrations increased, we note that the peak concentrations surpassing normal deposition clearly correlate with the sandy tsunami deposit, when present.

The peak isolongifolene concentration at location A6 (ca. 1×10^4 ng/g at 1–2 cm depth), where the sandy tsunami deposit is absent, probably represents the trace of the 2011 Tohoku-oki tsunami inundation (Fig. 5). At that location, we also observed elevated ^{137}Cs concentrations in the soil layer at 0–1 and 3–4 cm depth (Fig. 5), which we attribute to the aftermath of the Fukushima Daiichi Nuclear Power Plant incident in March 2011 and fallout from nuclear weapons testing in 1963, respectively (e.g., Marshall et al. 2007). Because the 2011 Tohoku-oki tsunami is the only large tsunami to have inundated this area since 1963, it is reasonable to conclude that the isolongifolene peak observed above the 1960s Cs peak at location A6 was caused by the tsunami. Similarly, we conclude that the peak isolongifolene concentration in the uppermost soil at location A7 also correlates with the 2011 Tohoku-oki tsunami inundation (Fig. 5).

5.3 Implications for precise estimation of tsunami inundation areas

Observations of the 1992 Flores (Shi et al. 1995), 2004 Sumatra (Chadha et al. 2005), and 2006 Kuril tsunamis (MacInnes et al. 2009) have demonstrated that seawater generally inundates areas beyond the distributions of associated visually identifiable sandy tsunami deposits. In Japan, Goto et al. (2011), Abe et al. (2012, 2020), Chagué-Goff et al. (2012), and Iijima et al. (2021) reported that the distributions of sandy tsunami deposits ≥ 0.5 cm thick were less extensive than the observed seawater inundation areas in the Tohoku region. Some studies have attempted to bridge this gap via geophysical approaches (Sugawara et al. 2011, 2013; Namegaya and Satake 2014), but it has proven too difficult to reconstruct past seawater inundation areas solely based on observations of stratigraphic records.

Our results indicate that geochemical approaches may be effective for identifying paleotsunami traces in geological layers beyond the limits of visually identifiable tsunami deposits. As with isolongifolene in the Oirase coastal pine forest, if an appropriate biogeochemical compound can be identified at a given study site, it could be used to reconstruct past tsunami inundation events (Fig. 5). Marine-sourced markers are known to be effective in identifying tsunami traces, and our results that even terrestrial-sourced markers can be used to identify tsunami traces add to the arsenal of techniques available. Although isolongifolene is likely restricted to pine forests and may not be useful in pine forests in other regions, our results suggest that it may be possible to detect tsunami inundation events by tracing depth and lateral changes of geochemical proxies specific to a given depositional environment, even if marine-sourced proxies are not present.

6 Conclusions

We performed sedimentological and geochemical investigations in a coastal pine forest that was inundated by the 2011 Tohoku-oki tsunami. Of the sites within the known inundation area, the sandy tsunami deposit was recognized at seaward sites, but was not visually or sedimentologically identifiable at the most landward sites. For comparison, we also studied a reference site beyond the known inundation limit. Marine-sourced biomarkers were absent at all locations, but isolongifolene, an organic compound derived from *Pinus*, was detected at all analyzed locations. Elevated isolongifolene concentrations clearly above the background soil concentration were observed not only within the sandy tsunami deposit, but also at similar depths in soil samples at locations further inland but still within the known inundation area; no peak isolongifolene concentration was observed at the reference site. These results suggest that the incorporation of this terrigenous biomarker into the soil was enhanced by or during the 2011 Tohoku tsunami inundation. Although the biological marker analyzed herein is probably unique to pine forests in Oirase, our results demonstrate that tsunami inundation events may be recorded as lateral and depth changes of terrestrial geochemical proxies specific to a given depositional environment.

Abbreviations

CT, Computed tomography; LOI, Loss on ignition; GC-MS, Gas chromatograph/mass spectrometer.

Declarations

Availability of data and material

Data sharing is not applicable to this article as no datasets were generated or analyzed during the current study. Please contact the corresponding author for data requests.

Competing interests

The authors declare that they have no competing interests.

Funding

This research was supported by Geological Survey of Japan (AIST) to YSa, DM, YSh, KT, TT) and a JSPS KAKENHI (20J00423) (to TS).

Authors' contributions

TS and YSa conceived and designed the study. TS, YSa, and DM conducted the field survey, and KT assisted with planning the field survey. TS and MI conducted biomarker analysis. TS conducted grain-size analysis, and DM analyzed the data. YSh conducted Cs analysis, and TT assisted with the interpretations. TS led the writing of the main text and preparation of the figures, with contributions from the other authors. All authors read and approved the final manuscript.

Acknowledgements

We acknowledge Kazumi Ito for his useful advice during Cs analyses. The biomarker analysis was performed under the cooperative research program of the Center for Advanced Marine Core Research (CMCR), Kochi University (Accept No. 20B067). CT image analysis was performed at the Geological Survey of Japan, AIST.

References

1. Abe T, Goto K, Sugawara D (2012) Relationship between the maximum extent of tsunami sand and the inundation limit of the 2011 Tohoku-oki tsunami on the Sendai Plain, Japan. Sediment Geol 282:142–150. https://doi.org/10.1016/j.sedgeo.2012.05.004
2. Abe T, Goto K, Sugawara D (2020) Spatial distribution and sources of tsunami deposits in a narrow valley setting – insight from 2011 Tohoku-oki tsunami deposits in northeastern Japan. Prog Earth

Planet Sci 7:1–21. https://doi.org/10.1186/s40645-019-0318-6

3. Atwater BF, Musumi-Rokkaku S, Satake K, Tsuji Y, Ueda K, Yamaguchi DK (2005) The orphan tsunami of 1700–Japanese clues to a parent earthquake in North America. USGS Professional Paper 1707. University of Washington Press, Seattle & London. https://doi.org/10.3133/pp1707.
4. Bellanova P, Frenken M, Nishimura Y, Schwarzbauer J, Reicherter K (2021) Tracing woody-organic tsunami deposits of the 2011 Tohoku-oki event in Misawa (Japan). Sci Rep 11:8947. https://doi.org/10.1038/s41598-021-88199-3
5. Chadha RK, Latha G, Yeh H, Peterson C, Katada T (2005) The tsunami of the great Sumatra earthquake of M 9.0 on 26 December 2004: impact on the east coast of India. Curr Sci 88:1297–1301
6. Chagué-Goff C, Goff J, Wong HKY, Cisternas M (2015) Insights from geochemistry and diatoms to characterise a tsunami's deposit and maximum inundation limit. Mar Geol 359:22–34. https://doi.org/10.1016/j.margeo.2014.11.009
7. Chagué-Goff C, Niedzielski P, Wong HKY, Szczuciński W, Sugawara D, Goff J (2012) Environmental impact assessment of the 2011 Tohoku-oki tsunami on the Sendai Plain. Sediment Geol 282:175–187. https://doi.org/10.1016/j.sedgeo.2012.06.002
8. Conte MH, Volkman JK, Eglinton G (1994) Lipid biomarkers of the Haptophyta. In: Green JC, Leadbeater BSC (eds) The Haptophyte Algae. Clarendon Press, Oxford, pp 351–377
9. Costa PJM, Dawson S, Ramalho RS, Engel M, Dourada F, Bosnic I, Andrade C (2021) A review on onshore tsunami deposits along the Atlantic coasts. Earth-Sci Rev 212:103441. https://doi.org/10.1016/j.earscirev.2020.103441
10. Dean WJ (1974) Determination of carbonate and organic matter in calcareous sediments and sedimentary rocks by loss on ignition: comparison with other methods. J Sediment Res 44:242–248. https://doi.org/10.1306/74D729D2-2B21-11D7-8648000102C1865D
11. Eglinton G, Hamilton RJ (1963) The distributions of alkanes. In: Swan T (ed) Chemical plant taxonomy. Academic Press, California, pp 187–217
12. Fujiwara O, Goto K, Ando R, Garrett E (2020) Paleotsunami research along the Nankai Trough and Ryukyu Trench subduction zones – Current achievements and future challenges. Earth-Sci Rev 210:103333. https://doi.org/10.1016/j.earscirev.2020.103333
13. Folk RL, Ward DC (1957) Brazos River bar: A study in the significance of grain size parameters. J Sediment Petrol 27:3–26. https://doi.org/10.1306/74D70646-2B21-11D7-8648000102C1865D
14. Goff J, Witter R, Terry J, Spiske M (2020) Palaeotsunamis in the Sino-Pacific region. Earth-Sci Rev 210:103352. https://doi.org/10.1016/j.earscirev.2020.103352
15. Goto K, Chagué-Goff C, Fujino S, Goff J, Nichimura Y, Richmond B, Sugawara D, Szczuciński W, Tappin DR, Witter RC, Yulianto E (2011) New insights of tsunami hazard from the 2011 Tohoku-oki event. Mar Geol 290:46–50. https://doi.org/10.1016/j.margeo.2011.10.004
16. He Q, Walling DE (1997) The distribution of fallout 137Cs and 210Pb in undisturbed and cultivated soils. Appl Radiat Isotopes 48:677–690. https://doi.org/10.1016/S0969-8043(96)00302-8

17. Iijima Y, Goto K, Sugawara D, Abe T (2021) Effect of artificial structures on the formation process of the 2011 Tohoku-oki tsunami deposits. Sediment Geol 423:105978. https://doi.org/10.1016/j.sedgeo.2021.105978
18. Jankaew K, Atwater BF, Sawai Y, Choowong M, Charoentitirat T, Martin ME, Prendergast A (2008) Medieval forewarning of the 2004 Indian Ocean tsunami in Thailand. Nature 455:1228–1231. https://doi.org/10.1038/nature07373
19. Koiwa N, Kasai M, Kataoka S, Isono T (2014) Examination of relation with tsunami behavior reconstructed from on-site sequence photographs, topography, and sedimentary deposits from the 2011 Tohoku-oki tsunami on the Kamikita Plain, Japan. Mar Geol 358:107–119. https://doi.org/10.1016/j.margeo.2014.08.009
20. MacInnes BT, Pinegina TK, Bourgeois J, Razhigaeva NG, Kaistrenko VM, Kravchunovskaya EA (2009) Field survey and geological effects of the 15 November 2006 Kuril tsunami in the middle Kuril Islands. In: Cummins PR, Satake K, Kong LSL (eds) Tsunami Science Four Years after the 2004 Indian Ocean Tsunami. Pageoph Topical Volumes. Birkhäuser Verlag, Basel, pp 9–36. https://doi.org/10.1007/978-3-0346-0064-4_2
21. Marlowe IT, Green JC, Neal AC, Brassell SC, Eglinton G, Course PA (1984) Long chain (n-C37–C39) alkenones in the Prymnesiophyceae. Distribution of alkenones and other lipids and their taxonomic significance. Brit Phycol J 19:203–216. https://doi.org/10.1080/00071618400650221
22. Marshall WA, Gehrels WR, Garnett MH, Freeman SPHT, Maden C, Xu S (2007) The use of 'bomb spike' calibration and high-precision AMS 14C analyses to date salt-marsh sediments deposited during the past three centuries. Quaternary Res 68:325–337. https://doi.org/10.1016/j.yqres.2007.07.005
23. Moreira S, Costa PJM, Andrade C, Lira CP, Freitas MC, Oliveira MA, Reichart G-J (2017) High resolution geochemical and grain-size analysis of the AD 1755 tsunami deposit: Insights into the inland extent and inundation phases. Mar Geol 390:94–105. https://doi.org/10.1016/j.margeo.2017.04.007
24. Mukai A, Takahashi K, Ashitani T (2017) Natural autoxidation of longifolene and anti-termite activities of the products. J Wood Sci 63:360–368. https://doi.org/10.1007/s10086-017-1637-0
25. Nakamura Y, Nishimura Y, Putra PS (2012) Local variation of inundation, sedimentary characteristics, and mineral assemblages of the 2011 Tohoku-oki tsunami on the Misawa coast, Aomori, Japan. Sediment Geol 282:216–227. https://doi.org/10.1016/j.sedgeo.2012.06.003
26. Namegaya Y, Satake K (2014) Reexamination of the A.D. 869 Jogan earthquake size from tsunami deposit distribution, simulated flow depth, and velocity. Geophys Res Lett 41:2297–2303. https://doi.org/10.1002/2013GL058678
27. Ozawa S, Nishimura T, Suito H, Kobayashi T, Tobita M, Imakiire T (2011) Coseismic and postseismic slip of the 2011 magnitude-9 Tohoku-Oki earthquake. Nature 475:373–376. https://doi.org/10.1038/nature10227
28. Paris R, Goto K, Goff J, Yanagisawa H (2020) Advance in the study of mega-tsunamis in the geological record. Earth-Sci Rev 210:103381. https://doi.org/10.1016/j.earscirev.2020.103381

29. Peters KE, Walters CC, Moldowan JM (2007) The Biomarker Guide volume 2: Biomarkers and Isotopes in Petroleum Exploration and Earth history. Cambridge University Press, Cambridge
30. Santisteban JI, Mediavilla R, López-Pamo E, Dabrio CJ, Zapata MBR, García JG, Castaño S, Martínez-Alfaro PE (2004) Loss on ignition: a qualitative or quantitative method for organic matter and carbonate mineral content in sediments? J Paleolimnol 32:287–299. https://doi.org/10.1023/B:JOPL.0000042999.30131.5b
31. Satake K, Atwater BF (2007) Long-term perspectives on giant earthquakes and tsunamis at subduction zones. Annu Rev Earth Planet Sci 35:349–374. https://doi.org/10.1146/annurev.earth.35.031306.140302
32. Sawai Y (2020) Subduction zone paleoseismology along the Pacific coast of northeast Japan – progress and remaining problems. Earth-Sci Rev 208:103261. https://doi.org/10.1016/j.earscirev.2020.103261
33. Sawai Y, Namegaya Y, Okamura Y, Satake K, Shishikura M (2012) Challenges of anticipating the 2011 Tohoku earthquake and tsunami using coastal geology. Geophys Res Lett 39:L21309. https://doi.org/10.1029/2012GL053692
34. Shi S, Dawson AG, Smith DE (1995) Coastal sedimentation associated with the December 12th, 1992 tsunami in Flores, Indonesia. Pure Appl Geophys 144:525–536. https://doi.org/10.1007/978-3-0348-7279-9_9
35. Shinozaki T (2021) Geochemical approaches in tsunami research: current knowledge and challenges. Geosci Lett 8:6. https://doi.org/10.1186/s40562-021-00177-9
36. Shinozaki T, Fujino S, Ikehara M, Sawai Y, Tamura T, Goto K, Sugawara D, Abe T (2015) Marine biomarkers deposited on coastal land by the 2011 Tohoku-oki tsunami. Nat Hazards 77:445–460. https://doi.org/10.1007/s11069-015-1598-9
37. Sugawara D, Imamura F, Matsumoto H, Goto K, Minoura K (2011) Reconstruction of the AD 869 Jogan earthquake induced tsunami by using the geological data. J JSNDS 29:501–516 (in Japanese with English abstract)
38. Sugawara D, Imamura F, Goto K, Matsumoto H, Minoura K (2013) The 2011 Tohoku-oki Earthquake Tsunami: Similarities and differences to the 869 Jogan Tsunami on the Sendai Plain. Pure Appl Geophys 170:831–843. https://doi.org/10.1007/s00024-012-0460-1
39. Tanigawa K, Sawai Y, Namegaya Y (2018) Diatom assemblages within tsunami deposit from the 2011 Tohoku-oki earthquake along the Misawa coast, Aomori Prefecture, northern Japan. Mar Geol 396:6–15. https://doi.org/10.1016/j.margeo.2016.11.016
40. The 2011 Tohoku Earthquake Tsunami Joint Survey Group (2011) Nationwide Field Survey of the 2011 Off the Pacific Coast of Tohoku Earthquake Tsunami. J Japan Soc Civil Eng Ser B 67:63–66. https://doi.org/10.2208/kaigan.67.63
41. Utsu T (2004) Catalog of Damaging Earthquakes in the World (through 2012). http//iisee.kenken.go.jp/utsu/index_eng.html

42. Volkman JK, Eglinton G, Corner EDS, Forsberg TEV (1980) Long chain alkense and alkenones in the marine coccolithophorid Emiliania huxleyi. Phytochemistry 19:2619–2622. https://doi.org/10.1016/S0031-9422(00)83930-8
43. Wren DG, Davidson GR (2011) Using lake sedimentation rates to quantify the effectiveness of erosion control in watersheds. J Soil Water Conserv 66:313–322. https://doi.org/10.2489/jswc.66.5.313

Figures

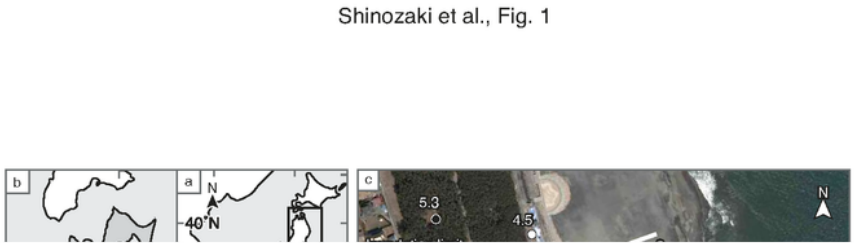

Figure 1

Location maps of the study site and topographic profiles of the studied transects. (a) Map of Japan. (b) Detail of east Japan showing the epicenter of the main shock of the 2011 M 9.0 Tohoku-oki earthquake (black star) and the associated coseismic slip distribution (dashed lines; Ozawa et al. 2011). (c) Aerial photograph of the study site in the coastal pine forest of Oirase. The inundation limit is inferred from eyewitness accounts and the debris distribution reported by Tanigawa et al. (2018). The run-up height

(the elevation at the most inland point inundated by the tsunami) and inundation height (the maximum inundation depth at a given point) are from The 2011 Tohoku Earthquake Tsunami Joint Survey Group (2011). (d, e) Topographic profiles and sampling locations along Transects A and B.

Figure 2

Photographs of the field survey. (a) A representative photograph of the study site, taken looking toward the ocean. (b) Excavated pit at location A2. (c) Sediment sample collected directly from the wall of the pit using a plastic sampling box.

Figure 3

Lithologic profiles along Transects A and B and at the reference location R. At each site, the stratigraphy is presented as (left) interpreted stratigraphic columns based on visual observations, and (center) photographs and (right) CT images of the sampled sediment columns.

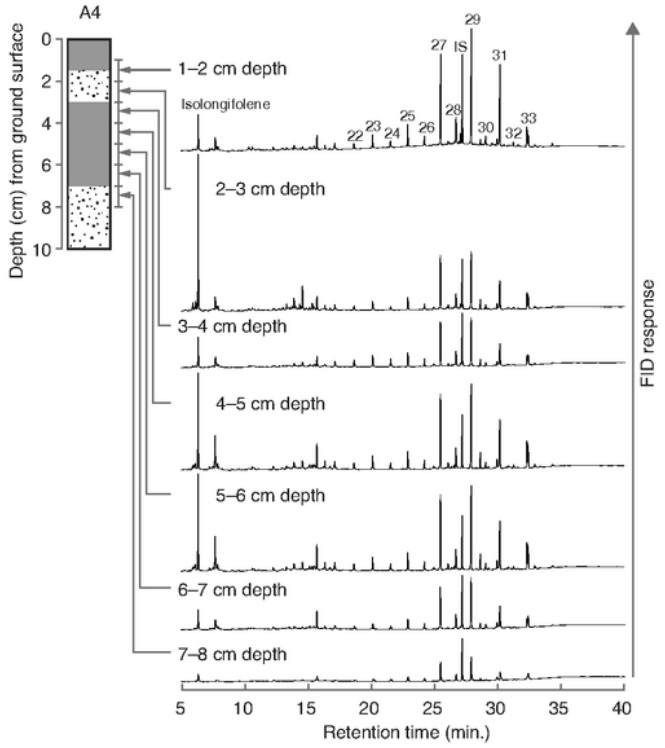

Figure 4

Gas chromatography of hydrocarbons (N1 fraction) at location A4. Numbers indicate *n*-alkanes (C_nH_{2n+2}) and 'IS' represents the 5α-cholestane internal standard. The retention time is the elapsed time at which the compound was detected. The flame ionization detector (FID) response represents signal intensity.

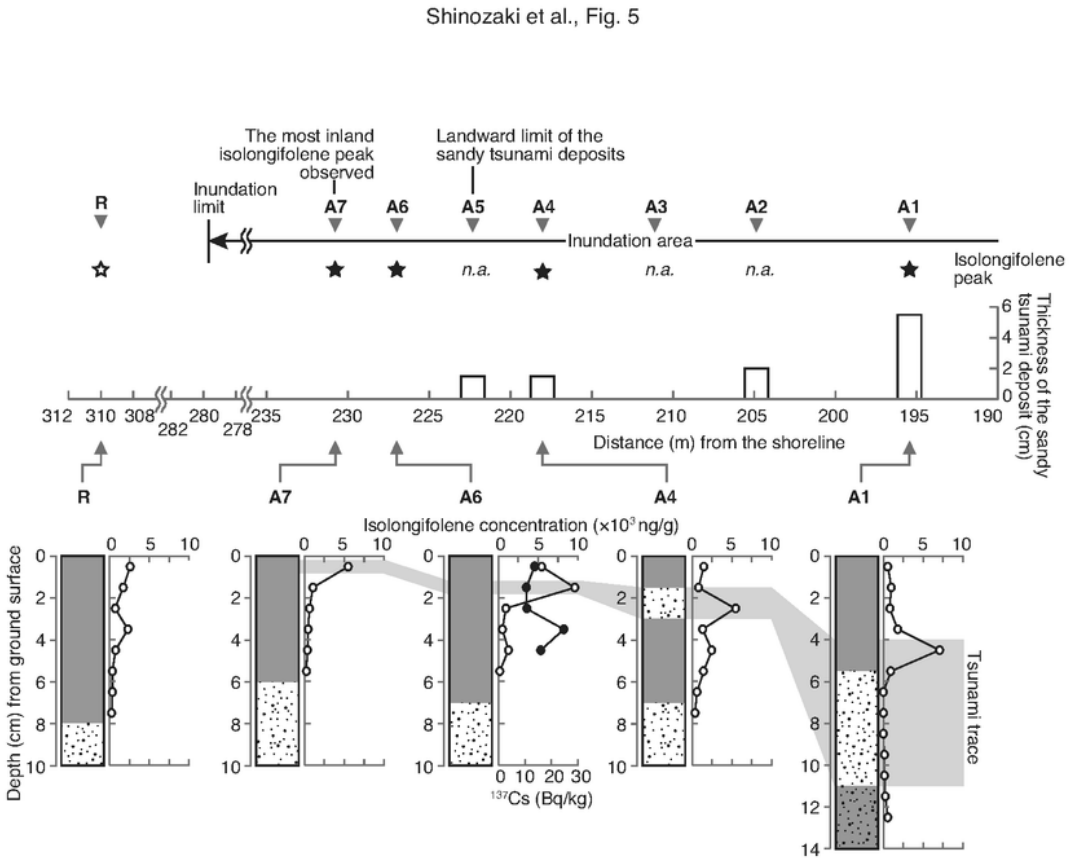

Figure 5

The thickness of the sandy tsunami deposit (bars), the presence/absence of isolongifolene concentration peaks (filled/open stars; *n.a.*, not analyzed), and stratigraphy based on visual observations and depth profiles of isolongifolene concentrations at locations A1, A4, A6, A7, and the reference site R (white circles), and ^{137}Cs concentrations at location A6 (black circles). The gray shaded area indicates our stratigraphic correlation of the tsunami trace, including the sand deposit and the isolongifolene peaks.

The black arrow representing the inundation area of the 2011 Tohoku-oki tsunami is based on Tanigawa et al. (2018).

Supplementary Files

This is a list of supplementary files associated with this preprint. Click to download.

- Fig.S1.pdf
- Fig.S2.pdf
- Fig.S3.pdf